

Article

# Bubble Dynamics during Laser Irradiated Thermo-Mechanical Response of Pigmented Skin Phantom

Jiafeng Wang and Bin Chen \* 

State key Laboratory of Multiphase Flow in Power Engineering, Xi'an Jiaotong University, Xi'an 710049, China; wangjiafeng@stu.xjtu.edu.cn

\* Correspondence: chenbin@mail.xjtu.edu.cn; Tel.: +86-29-8266-7326

**Abstract:** During the laser treatment of pigmented dermatosis such as Nevus of Ota, vapor bubbles will be generated by the laser with short pulse width and high energy density. Laser irradiation is efficacious for the clinical treatment of Ota's Nevus caused by hyperplasia of melanosomes in dermis. Since the mechanism of the laser–melanosome interaction is not yet clear, the clearance rate is generally low and bleeding of irradiated skin frequently occurs. This work conducted a flow visualization experiment to investigate the laser–melanosome interaction mechanism by using high-speed imaging. Pigmented phantom was prepared to simulate the diseased dermis tissue, where agar acted as substrate and synthetic melanin particles was infused as hyperplastic melanosomes. Putting the phantom into water, its thermo-mechanical responses to single-pulse 1064-nm Nd:YAG laser irradiation with energy density of 4~7 J/cm<sup>2</sup> and pulse duration of 6 ns were recorded. The results indicated that laser-induced bubble formation caused by the gasification of tissue moisture is the key mechanism of laser–melanosome interaction, and an optimal energy density of 6 J/cm<sup>2</sup> is recommended.

**Keywords:** bubble dynamic; gasification; melanosome; Nevus of Ota; thermo-mechanical damage; 1064-nm Nd:YAG laser



**Citation:** Wang, J.; Chen, B. Bubble Dynamics during Laser Irradiated Thermo-Mechanical Response of Pigmented Skin Phantom. *Energies* **2022**, *15*, 2019. <https://doi.org/10.3390/en15062019>

Academic Editors: Dmitry Eskin and Luiz C. Wrobel

Received: 26 January 2022

Accepted: 8 March 2022

Published: 10 March 2022

**Publisher's Note:** MDPI stays neutral with regard to jurisdictional claims in published maps and institutional affiliations.



**Copyright:** © 2022 by the authors. Licensee MDPI, Basel, Switzerland. This article is an open access article distributed under the terms and conditions of the Creative Commons Attribution (CC BY) license (<https://creativecommons.org/licenses/by/4.0/>).

## 1. Introduction

As a congenital skin lesion of blue-black or gray patches on the face, Nevus of Ota (NO) is a typical pigmented dermatosis caused by abnormality in melanocytes. The NO incidence in Asians is about 0.02–0.8%, with a 5:1 female-to-male ratio [1]. Normally, melanocytes will enter the dermis, immigrate to the stratum basale of the epidermis, move to the cuticle stratum corneum and fall out from the skin surface with a cycle of 28 days, as shown in Figure 1. However, in the case of NO, melanocytes will unnaturally retain in the dermis at the ophthalmic and maxillary branches of the trigeminal nerve and produce a large number of melanosomes, yielding nevus on the face [2,3]. This congenital pigmentation will accompany the patient for life and deepen with age, which will bring about considerable psychological problems and distress to patients.

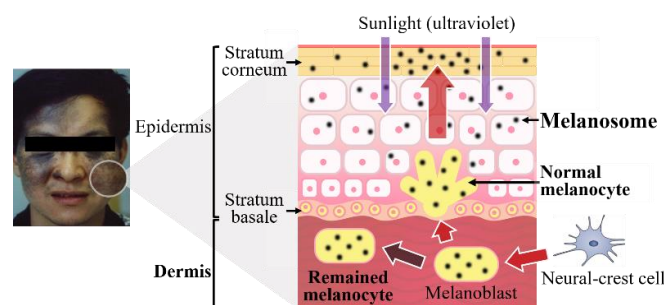


**Figure 1.** Migration of melanocytes.

Based on the theory of selective photothermolysis [4], laser irradiation has become a widely acknowledged strategy for the treatments of NO. The basic principle to bleach the skin is that melanosomes will be shattered and engulfed by macrophages via absorbing laser energy with appropriate wavelength and pulse duration. However, the clearance rates of NO lesions are unsatisfactorily low in general owing to experience-dependent therapy [5–7].

As shown in Figure 2, laser–tissue interaction can be divided into photo-chemical, thermal and thermo-mechanical processes [8]. At present, a Q-switched Nd:YAG laser with a wavelength of 1064 nm is commonly utilized in NO treatment [9,10]. According to the short pulse duration (ns to ps, even fs) and high-power density, the damage mechanism of melanosomes is not pure heat transfer but photoablation. Thermo-mechanical response occurs resulting in a heterogeneous energy distribution within the skin tissue. Rapid heating yields explosively expansion and breakup of melanosomes, which is a primarily mechanical damage. They are ablated in a short pulse duration before any heat is transferred to the surrounding tissue, while unexpected thermal damage can be avoided.

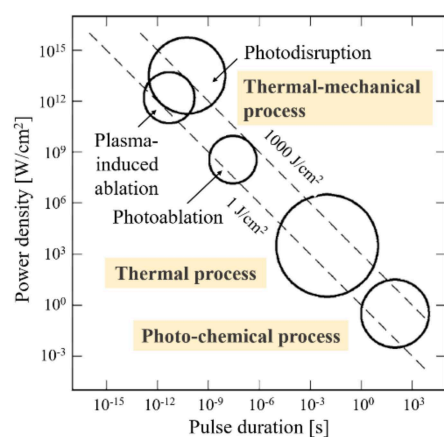


**Figure 2.** Pattern of laser–tissue interaction, adapted from [8].

However, the mechanism of laser–melanosome interaction is much more complicated. Biopsy specimens of NO immediately after laser irradiation show that the destruction of melanosomes differ in degree within large and tense round vacuoles [11]. In photoablation, micro-explosion of the melanosome makes surrounding moisture begin to flow instantaneously. The resulting partial depressurization causes the gasification of intracellular moisture to form in the cavitation bubble [12], which is different from the bubble formed around an undamaged melanosome, which is caused by the gasification of the intracellular moisture through heat conduction [13,14]. Whether the irradiated melanosomes are ablated, it can be speculated that the expansion and coalescence of bubbles produce tense round vacuoles larger than the original melanocytes. Although these vacuoles will disappear eventually, the refraction or scattering of the laser may have a serious influence on the absorption of laser energy by residual melanosomes during pulsed laser irradiation. In addition, for nanosecond pulse duration, the laser-induced expansion of the melanosomes is restricted by the surrounding tissue, leading to the generation of thermoelastic stresses and shock waves [15]. When shock waves propagate into the surrounding tissue, blood vessels or cells in the dermis tissue may be mechanically damaged. Accompanied by the side effects, such as bleeding, are often unavoidable [16]. The occurrence of bleeding will inhibit the increase in laser energy and even interrupt the laser irradiation. Therefore, the mechanism of laser–melanosomes interaction is necessary to be revealed to improve the efficiency and safety of laser irradiation.

Due to the difficulty of *in vivo* experiment, it is hard to visualize the transient interaction between laser and melanosomes during laser irradiation directly. Tissue phantoms have been widely used for the studies of optical, mechanical, and thermal properties of human skin. In this work, pigmented agar-based skin phantoms were prepared to simulate

the diseased dermis tissue. Hydrogel substance that are made from agar and water solution can simulate the layers of dermis tissue. Synthetic melanin is employed as the absorber in phantom because of the similar optical properties of human melanin [17]. The absorption and scattering of the agar hydrogel are usually neglected [18], so the laser energy is only absorbed by synthetic melanin particles. Most current laser–melanosome experiments focus on the thermal response of melanosomes but themselves. For example, Neumann and Brinkmann [13] irradiated melanosomes by ns-pulse laser irradiation. In this work, laser heating of the melanosomes results in vaporization of the surrounding liquid to form microbubbles around. In order to visually investigate the laser–melanosome interaction mechanism, the responses of pigmented phantom to single-pulse 1064-nm Nd:YAG laser irradiation were recorded by using high-speed imaging. The effects of energy density of laser irradiation on the responses were also explored.

## 2. Materials and Methods

Pigmented phantoms were produced using agar hydrogel and synthetic melanin particles. Agar hydrogel was made by mixing agar powder (A-7002, Sigma-Aldrich, St. Louis, MO, USA) with deionized water (Milli-RO60, Millipore, Burlington, MA, USA) and heating of the solution at temperature of 80 °C to simulate the ground substance of dermis. Two grams of synthetic melanin particles (diameter of 100–200 nm) were added to the solutions for simulating melanosomes. According to histological classification of NO [19], deionized water, agar powder, and synthetic melanin were thoroughly mixed in a mass ratio of 10:4:1. The density of particle in phantom is 0.09 g/cm<sup>3</sup>. The solutions were filled in cuboid plastic mould with an edge length of 3 cm and placed at room temperature to solidify. Under laser irradiation, synthetic melanin particles will be rapidly ablated, resulting in the gasification of moisture within the phantom to form cavitation bubbles.

An experimental system to visualize the underwater pigmented phantom during single-pulse 1064-nm Nd:YAG laser irradiation is shown in Figure 3. Backlight illumination method was implemented to record the responses of the phantom. A high-speed camera (Fastcam SA-Z, Photron, Tokyo, Japan) with a Macro lens (AF Micro-Nikkor 105 mm f/2.8 D, Nikon, Tokyo, Japan) was used to take the gray-scale photos at 100,000 fps with 150 × 400 pixels and exposure time of 1/800,000 s. A 120 W LED lamp was employed as the light source and a diffusing glass was employed in order to improve the uniformity of background illumination. A pulsed 1064-nm Q-switched Nd:YAG laser with energy density of 4–7 J/cm<sup>2</sup> and pulse duration of 6 ns was applied to irradiate the pigmented skin phantom vertically. An articulated arm was used to direct the laser beam.

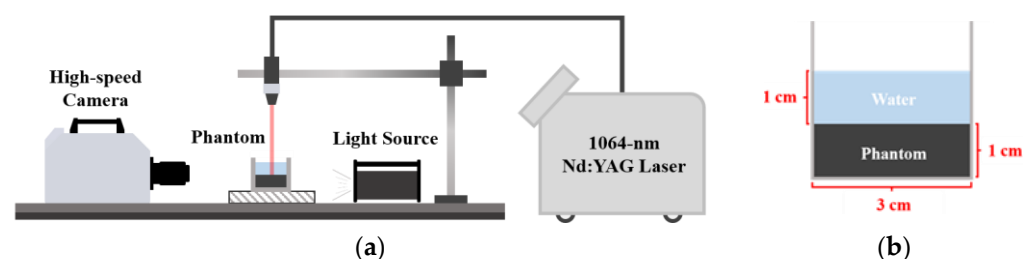


**Figure 3.** Schematic of experimental set-up: (a) Set-up; (b) underwater pigmented phantom.

In order to visualize the transient gasification of moisture within pigmented phantom, deionized water was filled into the mould to cover the surface of phantom and mimic the ground substance of dermis. The height of the phantom and the water are both 1 cm. A gray-scale image can be taken by the high-speed camera, as shown in Figure 4a. After binarization (Figure 4b), the bubble periphery can be extracted, as shown in Figure 4c.

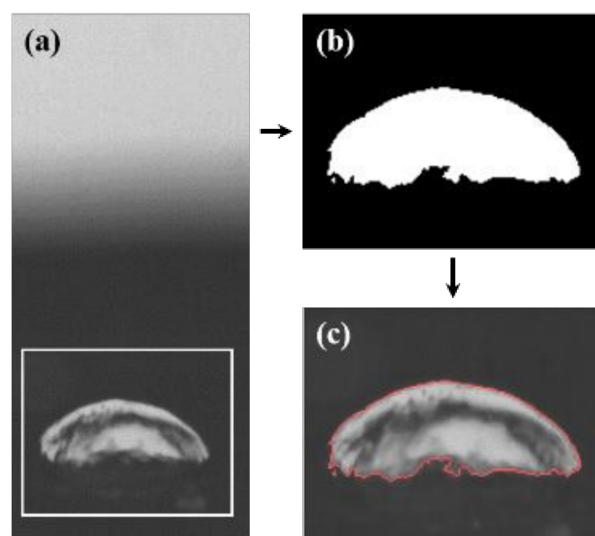


**Figure 4.** Image post processing procedure: (a) Gray-scale image; (b) Binarized image; (c) Periphery in red color.

### 3. Results and Discussion

#### 3.1. Thermo-Mechanical Response

The irradiation of the underwater pigmented phantom by single-pulse laser with a pulse duration of 6 ns at radiant exposures of  $5 \text{ J/cm}^2$  is presented in Figure 5. The dashed area in the first snapshot represents the laser irradiated surface of phantom, where the spot radius is 1 mm. The thermo-mechanical response is characterized by the ejection of very fine bubbles, as well as the generation, constriction, and collapse of a large bubble. During laser irradiation, synthetic melanin particles within the irradiated phantom are transiently shattered, and the surrounding moisture is rapidly gasified by laser energy absorption. These fine bubbles eject from the upper surface of the phantom into the water, forming a dense bubble flow at  $20 \mu\text{s}$ . This gasification induced by partial depressurization is so fast that almost no heat conduction occurs. High-pressure and high-temperature small bubbles are produced at a deep layer, thereafter coalescing to form a large bubble at the irradiated surface. With the attenuation of laser energy, synthetic melanin particles at deep layer may not be ablated, where the gasification induced by heat conduction may also occur. The threshold of energy density to gasify moisture by heat conduction is at the millijoule level, which is much lower than this work [12]. Owing to the high internal pressure, the large bubble gradually expands and rises. Instead of expanding to burst, the large bubble begins to shrink since the internal pressure is lower than the ambient pressure of free water. With the decrease in the internal pressure and temperature, the bubble collapses and detaches from the phantom surface at about  $310 \mu\text{s}$ . In the end, the pigmented phantom is bleached and a notch can be viewed at the center of the laser irradiation surface, as shown in Figure 5.

In this work, the laser–phantom interaction can be considered as photoablation according to the laser–tissue interaction pattern, as shown in Figure 2. Compared to the thermal process, photoablation causes far less thermal damage to the adjacent tissue. The absorption of the laser energy by melanin can mainly lead to a micro-explosion of synthetic melanin particles and the mechanical separation of the phantom. Histological features are in agreement with this photoablation process. The large bubble collapses, but the vacuoles remain in dermis because the ground substance of dermis has lower surface tension than water [15].

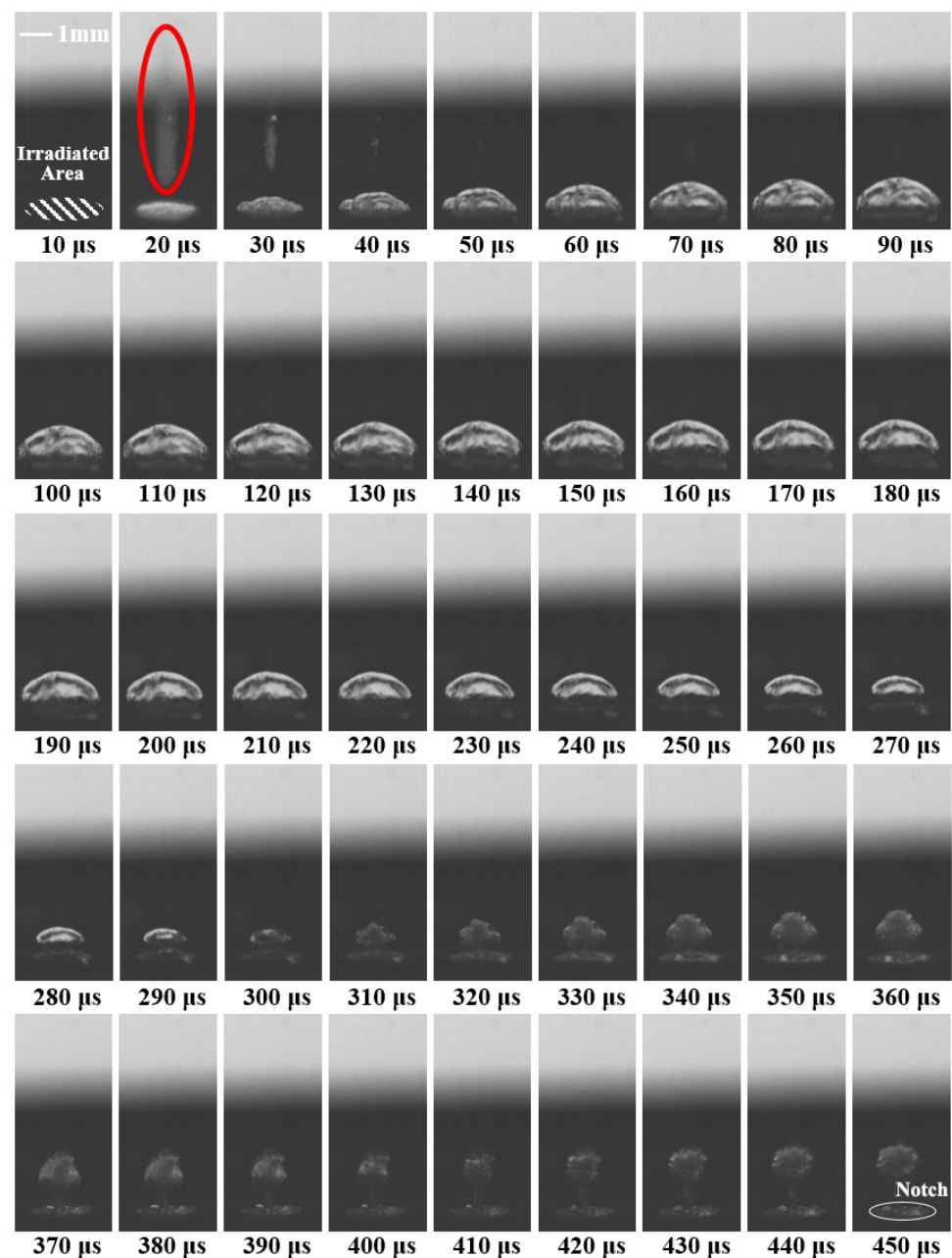


**Figure 5.** Dynamics responses of pigmented skin phantom to single-pulse 1064-nm laser irradiation with duration of 6 ns at radiant exposures of  $5 \text{ J/cm}^2$  (The dense bubble flow is labelled by the red circle).

### 3.2. Bubble Dynamic Measurement

The thermo-mechanical responses of the pigmented phantom to single-pulse 1064-nm laser irradiation suggest that the dynamics of the bubble formation is critical in the theoretical modelling of the laser–melanosome interaction. As shown in Figure 5, a large bubble begins to generate at about  $30 \mu\text{s}$  and collapses after  $300 \mu\text{s}$ . During this period, the dynamic variations in the horizontal length, vertical length, and area of the large bubble are calculated and displayed in Figure 6. In the early stage, the bubble expands with the time evolution. The largest area of  $1.06 \text{ mm}^2$  with a horizontal length of  $2.57 \text{ mm}$  and a vertical length of  $1.80 \text{ mm}$  occurs at the time of  $120 \mu\text{s}$  (point A). The expansion of the large bubble becomes slower because the internal pressure gradually decreases. When internal pressure is lower than the ambient pressure, the bubble continues to expand due to inertia. Afterwards, the bubble begins to shrink when the velocity of bubble surface

becomes zero. In terms of area variation, the average shrink rate of  $0.005 \text{ mm}^2/\mu\text{s}$  is lower than the average growth rate of  $0.007 \text{ mm}^2/\mu\text{s}$ .

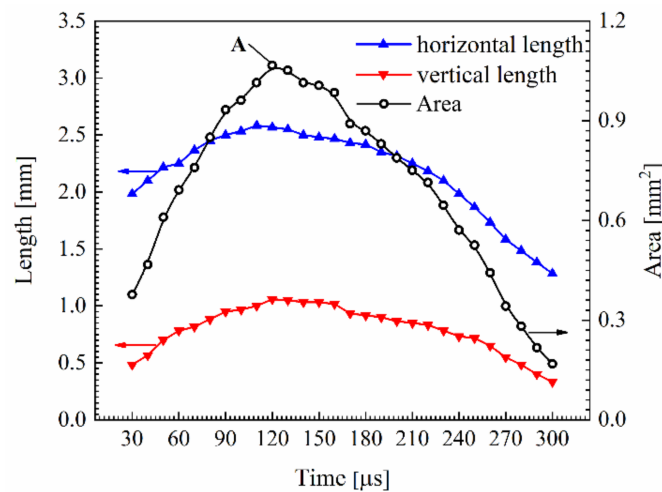


**Figure 6.** Size variation of large bubble.

In order to investigate the dynamic mechanism of the bubble formation at different laser irradiation conditions, single-pulse laser energy density is set from  $4 \text{ J/cm}^2$  to  $7 \text{ J/cm}^2$ . The existence durations ( $t$ ) of the large bubble at different laser energy density are counted and shown in Figure 7. It can be seen that the existence, growth, and shrinking duration of the large bubble all increase when the energy density increases. However, the three durations begin to decrease when the energy density is higher than  $6 \text{ J/cm}^2$ . The reason for this is that less bubbles remain in deeper layer forming a less persistent large bubble. To illustrate this, the effect of energy density ( $E$ ) on the largest area ( $A_{max}$ ) of dense bubble flow is demonstrated in Figure 8. The formations of dense bubbles followed by the generations of large bubbles are observed in all cases. When energy density increases, the area of the dense bubble flow increases, which means more synthetic melanin particles are ablated and more moisture gasifies to eject from the phantom surface. The  $A_{max}$  of the large bubble at different energy densities is also calculated in Figure 8. When  $E$  is lower than  $5.5 \text{ J/cm}^2$ , the increase in energy density results in greater quantity of the ejecting bubbles and broader expansion of the large bubble. At  $6 \text{ J/cm}^2$ ,  $A_{max}$  of large bubble becomes smaller than at  $5.5 \text{ J/cm}^2$  because the effect of energy density on the dense bubble flow begin to take a leading role. When the energy density is higher than  $6 \text{ J/cm}^2$ , not only the three durations but also the  $A_{max}$  of the large bubble decreases.

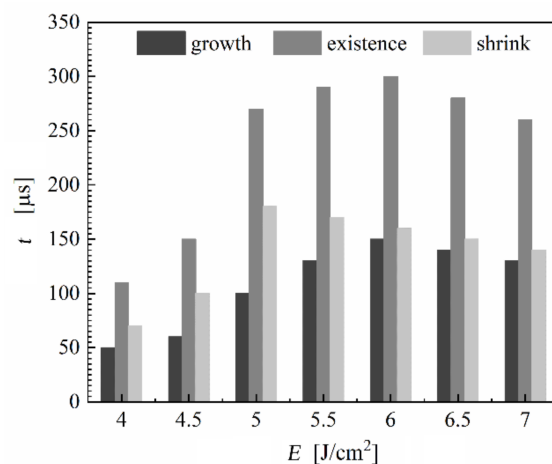


**Figure 7.** Effect of laser energy density on existence, growth and shrink duration.

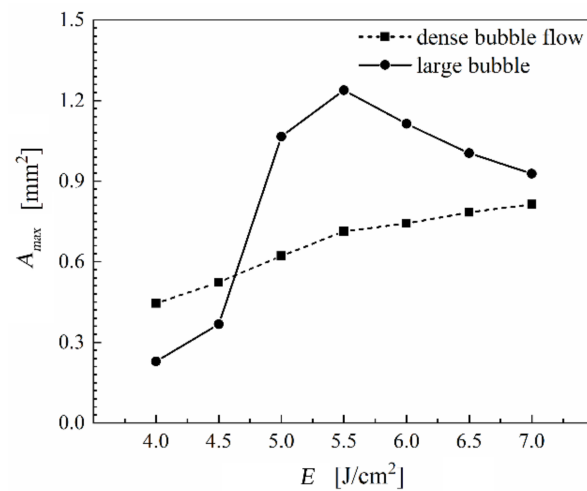


**Figure 8.**  $A_{max}$  of dense bubble flow and large bubble at different laser energy density.

The effect of energy density on the average area variation rate of the large bubble is shown in Figure 9. In accordance with Figure 8, the growth of the large bubble becomes faster and wider when energy density increases from 4 J/cm<sup>2</sup> to 5.5 J/cm<sup>2</sup>. The growth rate ( $s_g$ ) begins to decrease when the energy is higher than 6 J/cm<sup>2</sup>, owing to the lower internal pressure. The shrink rate ( $s_s$ ) has the same variation trend as shown in Figure 9. As can be seen in the figure, more synthetic melanin particles at superficial layer are ablated to form the dense bubble flow with the increase in the energy density. However, the penetration depth of laser irradiation is only related to wavelength in this work. When  $E$  is lower than 5.5 J/cm<sup>2</sup>, some melanin particles at deeper layer are ablated but maintain in the phantom. More bubbles caused by depressurization form the large bubble with the increase of energy density. On the contrary, less bubbles are formed attributing to heat conduction at deeper layer. By comparison, the former behaviour of the bubble formation is more intense. So, both  $s_g$  and  $s_s$  of the large bubble are higher with the increase in the energy density. When  $E$  is higher than 6 J/cm<sup>2</sup>, less ablated melanin particles are maintained with the increase in energy density, where  $s$  of the large bubble begins to decrease.

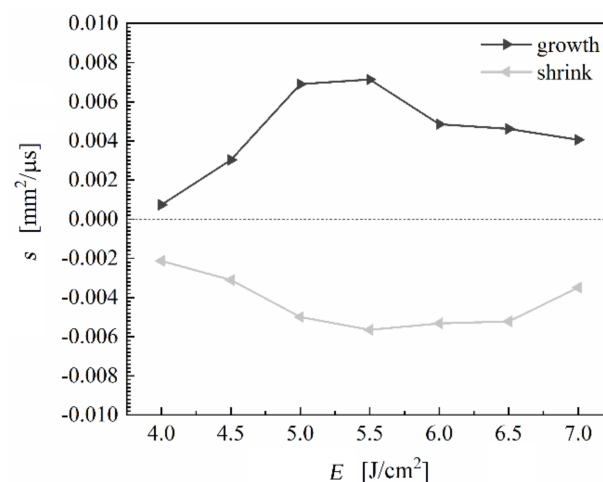


**Figure 9.** Growth and shrink rate of area at different laser energy density.

In the laser treatment of NO, the photoablation of hyperplastic melanosomes is desirable, but the accompanying damage of normal tissue should be avoided. With the increase in the laser's energy density, more intense shock waves are going to propagate, resulting in more mechanical damage to the skin tissue. In addition, the refraction or scattering of the laser caused by the bubbles should also be avoided. When laser energy is insufficient, the

residual melanosomes cannot be effectively ablated during pulsed laser irradiation because of the overformation of bubbles. Taking into account both efficiency and safety, 6 J/cm<sup>2</sup> is recommended as the optimal energy density to ablate melanosomes for the pulsed 1064-nm Q-switched Nd:YAG laser with a pulse duration of 6 ns.

#### 4. Conclusions

Laser-induced thermo-mechanical responses of pigmented phantom was investigated, which simulates the laser irradiation treatment of diseased dermis tissue of Ota's Nevus well. Owing to the absorption of the laser energy by melanin, synthetic melanin particles are transiently shattered at the phantom–water interface, yielding the gasification of moisture to form a dense bubble flow. Afterwards, bubbles within the phantom coalesce, followed by the generation, constriction, and collapse of a large bubble. The mechanism of the laser–melanosome interaction mainly reflects in the behavior of the bubble formation. When energy density increases, the photoablation of hyperplastic melanosomes becomes more effective, but the mechanical damage of the skin tissue may also increase. For the pulsed 1064-nm Q-switched Nd:YAG laser with pulse duration of 6 ns, the optimal energy density is 6 J/cm<sup>2</sup> in terms of efficiency and safety.

**Author Contributions:** Conceptualization, J.W. and B.C.; methodology, J.W. and B.C.; software, J.W.; validation, J.W. and B.C.; formal analysis, J.W.; investigation, J.W.; resources, J.W. and B.C.; data curation, J.W.; writing—original draft preparation, J.W.; writing—review and editing, J.W. and B.C.; visualization, J.W.; supervision, B.C.; project administration, B.C.; funding acquisition, B.C. All authors have read and agreed to the published version of the manuscript.

**Funding:** This research was funded by the National Natural Science Foundation of China, grant number 52036007, and the Fundamental Research Funds for the Central Universities.

**Conflicts of Interest:** The authors declare no conflict of interest.

#### References

1. Yu, P.; Yu, N.; Diao, W.; Yang, X.; Feng, Y.; Qi, Z. Comparison of clinical efficacy and complications between Q-switched alexandrite laser and Q-switched Nd: YAG laser on nevus of Ota: A systematic review and meta-analysis. *Lasers Med. Sci.* **2016**, *31*, 581–591. [[CrossRef](#)] [[PubMed](#)]
2. Mizoguchi, M.; Murakami, F.; Ito, M.; Asano, M.; Kubota, Y. Clinical, pathological, and etiologic aspects of acquired dermal Melanocytosis. *Pigment Cell Res.* **1997**, *10*, 176–183. [[CrossRef](#)] [[PubMed](#)]
3. Shah, V.V.; Bray, F.N.; Aldahan, A.S.; Mlacker, S.; Nouri, K. Lasers and nevus of Ota: A comprehensive review. *Lasers Med. Sci.* **2016**, *31*, 179–185. [[CrossRef](#)] [[PubMed](#)]
4. Anderson, R.R.; Parrish, J.A. Selective photothermolysis: Precise microsurgery by selective absorption of pulsed radiation. *Science* **1983**, *220*, 524–527. [[CrossRef](#)] [[PubMed](#)]
5. Chan, H.H.; Leung, R.S.; Ying, S.Y.; Lai, C.F.; Kono, T.; Chua, J.K.; Ho, W.S. A retrospective analysis of complications in the treatment of nevus of Ota with the Q-switched alexandrite and Q-switched Nd:YAG lasers. *Dermatol. Surg.* **2000**, *26*, 1000–1006. [[CrossRef](#)] [[PubMed](#)]
6. Chang, C.H.; Kou, C.S. Comparing the effectiveness of Q-switched ruby laser treatment with that of Q-switched Nd:YAG laser for oculodermal melanosis (Nevus of Ota). *J. Plast. Reconstr. Aesthetic Surg.* **2011**, *64*, 339–345. [[CrossRef](#)] [[PubMed](#)]
7. Aurangabadkar, S. QYAG5 Q-switched Nd:YAG laser treatment of nevus of Ota: An Indian study of 50 patients. *J. Cutan. Aesthetic Surg.* **2008**, *1*, 80–84. [[CrossRef](#)] [[PubMed](#)]
8. Luecking, M.; Brinkmann, R.; Ramos, S.; Stork, W.; Heussner, N. Capabilities and limitations of a new thermal finite volume model for the evaluation of laser-induced thermo-mechanical retinal damage. *Comput. Biol. Med.* **2020**, *122*, 103835. [[CrossRef](#)] [[PubMed](#)]
9. Choi, C.W.; Seo, H.M.; Kim, W.S. Beneficial effects of early treatment of Nevus of Ota with low-fluence 1064-nm Q-switched Nd:YAG laser. *Dermatol. Surg.* **2015**, *41*, 142–148.
10. Liu, Y.; Zeng, W.H.; Di, L.I.; Zhen, C.E.; Zhou, J.; Li, R.L.; Su, H. Clinical analysis of 1168 patients of Nevus of Ota. *Chin. J. Aesthetic Med.* **2018**, *27*, 60–62. [[CrossRef](#)]
11. Hakozaki, M.; Masuda, T.; Oikawa, H.; Nara, T. Light and electron microscopic investigation of the process of healing of the naevus of Ota by Q-switched alexandrite laser irradiation. *Virchows Arch.* **1997**, *431*, 63–71. [[CrossRef](#)] [[PubMed](#)]
12. Wang, S.P.; Zhang, A.M.; Liu, Y.L.; Zhang, S.; Cui, P. Bubble dynamics and its applications. *J. Hydrodyn.* **2018**, *30*, 975–991. [[CrossRef](#)]
13. Neumann, J.; Brinkmann, R. Boiling nucleation on melanosomes and microbeads transiently heated by nanosecond and microsecond laser pulses. *J. Biomed. Opt.* **2005**, *10*, 024001. [[CrossRef](#)] [[PubMed](#)]

14. Schmidt, M.S.; Kennedy, P.K.; Vincelette, R.L.; Denton, M.L.; Noojin, G.D.; Schuster, K.J.; Thomas, R.J.; Rockwell, B.A. Trends in melanosome microcavitation thresholds for nanosecond pulse exposures in the near infrared. *J. Biomed. Opt.* **2014**, *19*, 35003. [[CrossRef](#)] [[PubMed](#)]
15. Vogel, A.; Venugopalan, V. Mechanisms of pulsed laser ablation of biological tissues. *Chem. Rev.* **2003**, *103*, 577–644. [[CrossRef](#)] [[PubMed](#)]
16. Ge, Y.; Yang, Y.; Guo, L.; Zhang, M.; Wu, Q.; Zeng, R.; Rong, H.; Jia, G.; Shi, H.; Fang, J.; et al. Comparison of a picosecond alexandrite laser versus a Q-switched alexandrite laser for the treatment of nevus of Ota: A randomized, split-lesion, controlled trial. *J. Am. Acad. Dermatol.* **2020**, *83*, 397–403. [[CrossRef](#)] [[PubMed](#)]
17. Chen, A.I.; Balter, M.L.; Chen, M.I.; Gross, D.; Alam, S.K.; Maguire, T.J.; Yarmush, M.L. Multilayered tissue mimicking skin and vessel phantoms with tunable mechanical, optical, and acoustic properties. *Med. Phys.* **2016**, *43*, 3117–3131. [[CrossRef](#)] [[PubMed](#)]
18. Kuzmina, I.; Lukinsone, V.; Rubins, U.; Osina, I.; Spigulis, J. Agar-based phantoms for skin diagnostic imaging. *Tissue Opt. Photonic* **2020**, *11363*, 113630F.
19. Hirayama, T.; Suzuki, T. A new classification of Ota's nevus based on histopathological features. *Dermatology* **1991**, *183*, 169–172. [[CrossRef](#)] [[PubMed](#)]